polycrystalline hafnium-metal absorber were found to have relative intensities of $(0.36\pm0.12):1:1$, which suggests that the Debye-Waller factor is somewhat anisotropic; but because of the uncertainty in the intensity estimate, no definite conclusion can be drawn. The FWHM of the Mössbauer lines with the single-crystal absorbers were found to be 3.2 ± 0.1 mm/sec for the γ rays propagating parallel to the c axis and 2.67 ± 0.14 mm/sec for the γ rays propagating perpendicular to the c axis. Since η is practically zero, the broadening of these Mössbauer lines must be attributed entirely to the effective thickness of the absorbers. The observed broadenings correspond to Debye temperatures of (227 ± 10)°K for the γ rays propagating along the c axis and (192 ± 13)°K for the γ rays propagating perpendicular to the c axis.

ACKNOWLEDGMENTS

Our grateful thanks are due to Miss Ruth Mary Larimer of the Lawrence Radiation Laboratory, Berkeley, for her kindness in providing many sources of W^{178} and to Professor Donald F. Gibbons for putting the facilities of the Center for the Study of Materials at our disposal. Dr. W. R. Owens started the Mössbauer-effect studies in Hf^{178} in this laboratory.

PHYSICAL REVIEW VOLUME 187, NUMBER 2 10 NOVEMBER 1969

Alpha-Particle Stopping Cross Section in Solids from 400 keV to 2 MeV†

W. K. Chu and D. Powers
Baylor University, Waco, Texas 76703

(Received 20 May 1969; revised manuscript received 14 July 1969)

Stopping cross sections of α particles from 400 keV to 2 MeV have been measured to an accuracy of ±3.6 to $\pm4.9\%$ in 17 elements (Be, C, Mg, Al, Ti, V, Cr, Mn, Fe, Co, Ni, Cu, Ge, Pd, Ag, In, and Sn). The experimental method consists of the elastic scattering of α particles from a thick Ta backing onto which a thin layer of target element has been evaporated. The energy loss of α particles in the target film is determined by the difference in energy between α particles scattered from clean Ta and α particles scattered from Ta after having gone through the thin layer of target element. The results are compared with measurements by Porat and Ramavataram and by Gobeli and with estimates by Whaling; the discrepancies range from 1 to 20%. Structure in and a decrease of the α-particle stopping cross section ϵ_α with stopping element atomic number Z_2 are noticed in the region $Z_2=22$–29. This dependence is not predicted by the Bethe-Bloch formalism valid at higher velocities, nor by the Firsov or the Lindhard formalism valid at lower velocities. The oscillatory structure of ϵ_α on Z_2 is discussed qualitatively by comparing $\epsilon_\alpha(E_\alpha)$ versus Z_2 with a Hartree-Fock-Slater potential $\phi(r)$ versus Z, with E_α related to the radius r by a velocity comparison. An empirical formula for $\epsilon_\alpha=\epsilon_\alpha(E_\alpha,Z_2)$ has been constructed from the present measurements.

I. INTRODUCTION

In 1963 Ormrod and Duckworth[1] discovered that the electronic stopping cross section ϵ_{ion} has an oscillating dependence on Z_{ion}. This oscillatory dependence (or periodic structure) of ϵ_{ion} on Z_{ion} has been verified at low energies in boron, carbon, and aluminum thin films[2,3] and in gaseous media[4,5] at higher energies (0.1–1.5 MeV) and $Z_{\text{ion}}\lesssim39$ in thin carbon films,[6,7] and has also been verified in the channeling of heavy ions in oriented W single crystals[8] and Si crystals.[9] This oscillating phenomenon is of interest in that it was not predicted by the theories of Firsov[10] or of Lindhard, Scharff, and Schiøtt[11] applicable in the low-velocity region of the incident ion. Several theoretical treatments[12] obtaining Z_{ion} oscillations from Hartree-Fock wave functions have recently been made. El-Hoshy and Gibbons[13] have correlated the periodic structure with electronic shell structure of the atoms. These treatments modify Firsov's or Lindhard's formalism in one way or another, and the authors successfully interpret the ϵ_{ion}

† Research supported in part by the National Science Foundation.

[1] J. H. Ormrod and H. E. Duckworth, Can. J. Phys. **41**, 1424 (1963).

[2] J. H. Ormrod, J. R. MacDonald, and H. E. Duckworth, Can. J. Phys. **43**, 275 (1965).

[3] J. R. MacDonald, J. H. Ormrod, and H. E. Duckworth, Z. Naturforsh. **21a**, 130 (1966).

[4] B. Fastrup, A. Borup, and P. Hvelplund, Can. J. Phys. **46**, 489 (1968).

[5] J. H. Ormrod, Can. J. Phys. **46**, 497 (1968).

[6] B. Fastrup, P. Hvelplund, and C. A. Sautter, Kgl. Danske Videnskab. Selskab, Mat.-Fys. Medd. **35**, No. 10 (1966).

[7] P. Hvelplund and B. Fastrup, Phys. Rev. **165**, 408 (1968).

[8] L. Eriksson, J. A. Davies, and P. Jespergaard, Phys. Rev. **161**, 219 (1967).

[9] F. H. Eisen, Can. J. Phys. **46**, 561 (1968).

[10] O. B. Firsov, Zh. Eksperim. i Teor. Fiz. **36**, 1517 (1959) [English transl.: Soviet Phys.—JETP **9**, 1076 (1959)].

[11] J. Lindhard, M. Scharff, and H. Schiøtt, Kgl. Danske Videnskab. Selskab, Mat.-Fys. Medd. **33**, No. 14 (1963).

[12] I. M. Cheshire, G. Dearnaley, and J. M. Poate, Phys. Letters **27A**, 304 (1968); C. P. Bhalla and J. N. Bradford, *ibid.* **27A**, 318 (1968); K. B. Winterbon, Can. J. Phys. **46**, 2429 (1968).

[13] A. H. El-Hoshy and J. F. Gibbons, Phys. Rev. **173**, 454 (1968).

measurements by Eriksson *et al.*[8] in oriented W single crystals and by Eisen in Si crystals.[9]

The present experiment is different from the above-mentioned experiments in two respects: (1) The above experiments are performed for a given target element by varying the projectile Z_{ion} to study the dependence of the stopping cross section on Z_{ion}. The present experiment uses a fixed ion (α particle) with different target elements to study the dependence of ϵ_{ion} on Z_{targ}. (2) The present experiment is performed at an intermediate ion velocity where the velocity of the projectile is of the same order of magnitude as the velocity of the least-tightly bound electrons of the stopping medium. No theory of the stopping process exists in this velocity region. The purpose of the present experiment is to measure α-particle stopping cross sections in various elements and at energies not previously reported and to see if a periodic structure exists in the dependence of ϵ_{ion} on Z_{targ}.

II. EXPERIMENTAL METHOD AND ANALYSIS

The experimental method was developed by Warters[14] for finding the stopping cross section of protons in Li. The technique is applied in the present experiment to measure the stopping cross section of α particles in various substances. The experimental procedure consists in evaporating a thin uniform layer of substance onto part of a known area of thick polished Ta backing. The thickness of the target ($\rho\Delta x$ in μg/cm^2) is determined by weighing with a precision microbalance the backing before and after vacuum deposition. α particles are then elastically scattered from the Ta backing and from the Ta-plus-target area to determine the energy loss of α particles in the coated film.

The experimental arrangement is similar to that used for previous range measurements[15,16] made in this laboratory with a 2-MeV electrostatic accelerator. An 18-in. scattering chamber with solid-state detector is used for detecting the scattered α particles. The signal from the detector goes through a preamplifier, linear amplifier, biased amplifier and enters a 200-channel analyzer with digital printout. The detecting system is calibrated with a mercury pulser.

Figure 1 gives a diagram of the scattering geometry and the corresponding energy profiles for the scattered α particles from clean Ta and from Ta after having gone through the thin layer of target element (in this case, vanadium). E_{1B} is the energy of the incident α particle. E_{2B} is the energy of the α particles scattered from the Ta surface, where by conservation of kinetic energy and

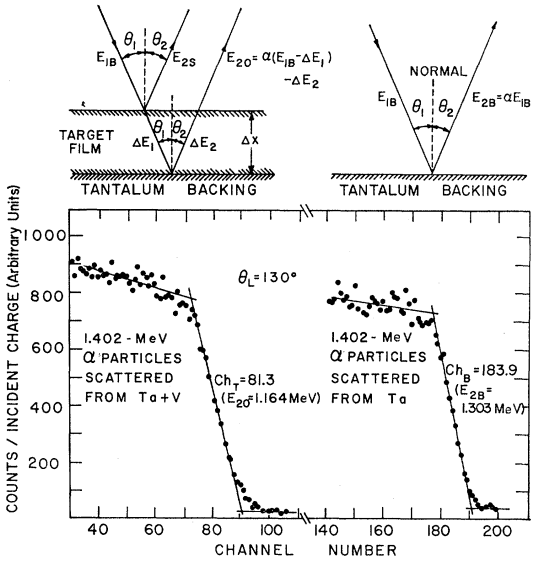

FIG. 1. Typical example of the scattering kinematics and the corresponding energy profiles for the scattered α particles. $\theta_1=\theta_2=25°$, $\theta_L=130°$, and $\rho\Delta x=59.6$ μg/cm^2. $E_{1B}=1.402$ MeV is the incident beam energy, $E_{2B}=\alpha E_{1B}=1.303$ MeV is the energy of the α particles scattered from the clean Ta surface corresponding to the step of the profile ($Ch_B=183.9$). E_{20} is the energy of the α particles scattered from the Ta after having gone through the thin vanadium film. $E_{20}=1.164$ MeV, corresponding to the step of the profile at channel number 81.3, is calculated from the profile step number ($Ch_T=81.3$) by a channel-to-voltage and voltage-to-energy calibration. The shift of the step corresponds to the energy loss $\Delta E=E_{2B}-E_{20}=139$ keV.

momentum we have

$$E_{2B}=\alpha E_{1B}, \tag{1}$$

with

$$\alpha=\alpha(M_1,M_{2'},\theta_L)=\left\{\frac{M_1\cos\theta_L}{M_1+M_{2'}}+\left[\left(\frac{M_1\cos\theta_L}{M_1+M_{2'}}\right)^2+\frac{M_{2'}-M_1}{M_{2'}+M_1}\right]^{1/2}\right\}^2. \tag{2}$$

M_1 is the mass of the α particle, $M_{2'}$ is the mass of the Ta atom, and θ_L ($=130°$) is the laboratory scattering angle. θ_1 ($=25°$) is the angle between the normal and the incident α-particle beam of energy E_{1B}. θ_2 ($=25°$) is the angle between the normal and the scattered α-particle beam of energy E_{2B}. E_{20} is the energy of α particles scattered from the Ta surface after having gone through the V thin film. The energy difference $\Delta E=E_{2B}-E_{20}$ is the energy loss of the α particles in going through the V film. This energy difference is obtained from the step shift of the corresponding profiles with a calibration which is established from the mercury pulser voltage and scattering kinematics. Several pulses of known voltages from the pulser are fed into the multichannel analyzer to obtain a voltage–versus–channel-number relation. This relation allows one to translate the channel number of each profile step into a voltage reading. The E_{2B} from Eq. (1) corre-

[14] W. D. Warters, Ph.D. thesis, California Institute of Technology, 1953, p. 38 (unpublished).

[15] D. Powers, W. K. Chu, and P. D. Bourland, Phys. Rev. **165**, 376 (1968).

[16] W. K. Chu, P. D. Bourland, K. H. Wang, and D. Powers, Phys. Rev. **175**, 343 (1968).

sponds to a voltage reading obtained from the linear voltage–versus–channel-number curve. Scattering of α particles from the Ta surface at different accelerator energies enables one to construct a linear relation between scattered α-particle energy and pulser voltage by the least-squares method. All pulser voltage readings are then converted to α-particle energies from this curve.

The stopping cross section of α particles in a given target material is then given by[14]

$$\epsilon_\alpha(E_x)=\frac{M_2\cos\theta_1}{N_0(\alpha+1)}\frac{(E_{2B}-E_{20})}{\rho\Delta x}, \quad (3)$$

where $\theta_1=\theta_2$, N_0 is Avogadro's number, and M_2 is the particle mass of the stopping element. E_x is an intermediate energy of the α particle in the coated layer, given by Warters as[14]

$$E_x=\frac{E_{2B}+E_{20}}{\alpha+1}+\frac{E_{2B}-E_{20}}{2(\alpha+1)}\frac{\eta-\alpha}{\eta+\alpha}, \quad (4)$$

where η is defined as $\epsilon_\alpha(E_{20})/\epsilon_\alpha(E_{1B})$, the ratio of the α-particle stopping cross section at E_{20} to that at E_{1B}.

III. TARGET PREPARATION

The preparation consisted of vacuum evaporation of a target element onto a highly polished Ta backing. Ta was selected since it is desirable to have a backing with somewhat higher mass number than the mass number of the coating substance, or else the magnitude of E_{2B} will be close to that of E_{2S} (see Fig. 1), and large uncertainties will be introduced in the energy determination. Throughout the experiment 0.005-in. Ta foils with a bright Zendiner finish from Fansteel Metallurgical Corp., Chicago, Ill., were used. Each Ta blank was cut into a 1×2-in. piece and polished with Wenol metal polishing compound, and then washed thoroughly with acetone, distilled water, liquid soap, and again with distilled water several times. After the Ta blank was cleaned and dried, it was weighed carefully on a Mettler M-5 microbalance. Five weighings were made each time, and their results were averaged. The Ta blank was then sandwiched between two pieces of Al plate. One of the Al plates which covered the polished Ta surface had a circular opening of 2.85 cm². This area was chosen to provide sufficient weight of deposited material to minimize the percentage error in the weighing technique as well as to provide space for several different beam positions on the target so that several $dE/\rho dx$ measurements could be made with the same target. Target elements were then deposited by vacuum evaporation onto the Ta backing within the above-mentioned area. After deposition, the weighing process was repeated and the thickness of the target was calculated.

Seventeen research-grade high-purity elements were used for targets in this experiment. They were Be obtained from Brush Beryllium Co., Cleveland, Ohio; C obtained from Ringsdorff Werke GmbH. Mehlem, Rhein, Germany; Ni obtained from Chromium Corp. of America, Waterbury, Conn.; and Mg, Al, Ti, V, Cr, Mn, Fe, Co, Cu, Ge, Pd, Ag, In, and Sn obtained from A. D. Mackay, Inc., New York, N. Y.

The evaporating techniques and refractory support materials for evaporating targets depend on the melting points, alloying ability, evaporation rate, etc. Refractory support materials were obtained from R. D. Mathis, Co., Long Beach, Calif. Holland's guide[17] was used for preparing the thin films.

Fifty-six targets of different thickness were used in this experiment. For each element at least two targets of different thicknesses were used to show that the stopping–cross-section measurements were independent of the target thickness used. The thicknesses varied from 13.4 μg/cm² (one of the Be targets) to 184 μg/cm² (one of the Sn targets), and most of the targets had thicknesses of 30–90 μg/cm².

IV. TESTS OF EXPERIMENTAL PROCEDURE

A. Spectrometer Test

Stopping cross sections of α particles in Al were measured at 0.5, 0.8, 1.1, 1.4, and 1.7 MeV by analyzing in a 60° spectrometer the He^+ and He^{++} beams emerging from the Al coating. The measurements with He^+ and He^{++} agreed within experimental accuracy as anticipated since charge equilibrium had been established by the time the scattered He beam emerged from the Al. Although $dE/\rho dx$ was measured by detecting, say, He^{++} with the 60° magnetic spectrometer, this does not mean that $dE/\rho dx$ of He^{++} was measured in the target. The charge-exchange process is a random process, and the measured $dE/\rho dx$ is actually an average value of the energy loss of all different charge states of the He ions. The counting rates of the He^+ and He^{++} ions emerging from the target at 1.4 MeV were compared, and the He^+-to-He^{++} scattering-cross-section ratio was observed to be about 1 to 8, a charge fraction in fair agreement with the prediction of 1 to 7 reported in *Nuclear Data Tables*.[18]

The $dE/\rho dx$ measurements in Al with 60° magnetic spectrometer agreed with those obtained from the solid-state detector within experimental accuracy, thereby indicating that the energy measurements were consistent.

B. Other Tests

The geometry of the scattering chamber was carefully checked. A range measurement of oxygen in Be

[17] L. Holland, *Vacuum Deposition of Thin Films* (Chapman and Hall Ltd., London, 1963).

[18] J. B. Marion, *1960 Nuclear Data Tables* (U. S. Government Printing Office, Washington, D. C., 1960), Part 3, Fig. 12.

was made at both +130° and −130° lab scattering angles. The agreement of these range measurements indicated that the angles +130° and −130° were symmetric with respect to the 0° reference position. Most of the α-particle stopping-cross-section measurements were made at +130°. The measurements in Ni and Co were made at both 130° and 90°, and the measurements in Fe were made at 90°, 130°, and 160° in order to check the scattering geometry. The agreement of these stopping-cross-section measurements within experimental accuracy proved the measurements to be independent of scattering angle and also provided a check on the scattering-chamber geometry.

The uniformity of each target was checked as follows: α particles of the same energy were scattered from three different spots on each target coating to determine if the midpoint of the steps (see Fig. 1) remained essentially at the same channel. The agreement within ±2 channels in all cases indicated that the target was uniform within ±2%, since the separation of the midpoint of the backing step from the midpoint of the target-plus-backing step was always around 100 channels. The accuracy of reading the midpoints depended on the resolution of the step; this resolution is a function of target thickness for target-plus-backing profile. Targets of uniformity worse than ±2% were discarded and not used in the experiment.

Tests were also made of the scattering-chamber detecting electronics during each stopping-cross-section measurement by monitoring the shape and height of the pulses to ensure that the pulses were not distorted by improper gain, bias level, and voltage settings. Stopping-cross-section measurements were also made by using different detectors, different preamplifiers, and different biased amplifiers with all kinds of combinations. The agreement of the measurements within experimental accuracy proved the measurements to be independent of the electronics equipment used.

A linearity test of the electronics system was made by feeding eight pulses at different voltages into the preamplifier to cover all channels of the multichannel analyzer used in the experiment. A voltage–versus–channel-number plot indicated the linearity to be good to one channel. Both long-term and short-term stability tests of the electronics were also made during the experiment, and the over-all stability of the detecting system was better than one channel.

V. ACCURACY

The sources of experimental error are listed in Table I, where the first column gives the parameter entering the stopping-cross-section calculation, the second column gives the probable error in each parameter, and the third column gives the error contribution to the stopping calculation. The case given in Table I is the probable error of the α-particle stopping-cross-section measurement in Ag, but the result is typical for all targets used in the experiment, although the values for different targets may fluctuate somewhat about these values because of the target thickness used. There is generally a decreasing percent of error with thicker target. The effect of each error is obtained by independently varying the appropriate parameter which appears in the calculation for the stopping cross section [Eq. (3)]. The over-all uncertainty in the measurement of α-particle stopping cross section in solids varies from 3.6 to 4.9%.

TABLE I. Experimental accuracy of the α-stopping cross-section measurement in Ag. ($\theta_1=25°$, $\theta_L=130°$, $\rho\Delta x=49.8$ μg/cm².)

	Source of error	Probable error in source	Probable error in ε from this source
θ_1	Uncertainty in incident angle	0.3°	0.24%
θ_L	Uncertainty in scattering angle	0.3°	0.01%
$\rho\Delta x$	Uncertainty in film thickness due to		
	(i) uniformity of film	2.0%	2.0 %
	(ii) uncertainty in coating area	1.6%	1.6 %
	(iii) uncertainty in weighing	1.3 μg	0.92%
ΔE	Uncertainty in energy loss due to		
	(i) uncertainty in midpoints of the steps	1.61 channels	2.03%
	(ii) uncertainty in pulser calibration	1.5%	1.5 %
	(iii) stability of electronics	1.0%	1.0 %
	(iv) linearity of electronics	1.5%	1.5 %
	(v) uncertainty in scattering energy due to uncertainty in θ_L	0.3°	0.01%
	(vi) uncertainty in incident energy E_{1B}	0.3%	0.3 %
	Root-mean-square probable error:		4.2 %

VI. RESULTS

The experimental results are tabulated as a function of the energy in Table II and are plotted in Figs. 2 and 3. In these figures are included Porat and Ramavataram's $dE/\rho dx$ measurements[19] (±5% accuracy) of α particles in C, Al, Ni, and Ag. The inverted triangles with ±10% accuracy in Figs. 2 and 3 are obtained by differentiating[20] the range measurements of Gobeli.[21] The squares (called Whaling's estimate in the present discussion) are $dE/\rho dx$ values of α particles in a given material as calculated by Whaling[20] from the effective charge of α particles and the $dE/\rho dx$ of protons[22] in the same stopping material at the same velocity as the α particles.

The dashed lines in Figs. 2 and 3 are obtained by a least-squares fit of a portion of the present measurements to a curve of the form $\epsilon_\alpha=(A/E)\ln(BE)$. The

[19] D. I. Porat and K. Ramavataram, Proc. Phys. Soc. (London) **78**, 1135 (1961).

[20] W. Whaling, in *Handbuch der Physik*, edited by S. Flügge (Springer-Verlag, Berlin, 1958), Vol. 34, p. 193.

[21] G. W. Gobeli, Phys. Rev. **103**, 275 (1956).

[22] The proton stopping measurements were done by several groups [M. Bader, R. E. Pixley, F. S. Mozer, and W. Whaling, Phys. Rev. **103**, 32 (1956); D. W. Green, J. N. Cooper, and J. Harris, *ibid.* **98**, 466 (1955); H. K. Reynolds, D. N. F. Dunbar, W. A. Wenzel, and W. Whaling, *ibid.* **92**, 742 (1953)] and reviewed by W. Whaling (see Ref. 20).

TABLE II. Energy loss of α particles in various stopping materials. Column 1: stopping material in order of increasing atomic number, along with the averaged percentage probable error. Column 2: α-particle energy [E_x of Eq. (4)]. Column 3: energy loss in keV cm^2/μg. Column 4: stopping cross section ϵ_α in 10^{-15} eV cm^2.

Stopping material	Energy (keV)	$dE/\rho dx$ (keV cm^2/μg)	ϵ (10^{-15} eV cm^2)
Be (4.9%)	459.4	1.81	27.0
	603.0	1.79	26.8
	740.0	1.74	26.1
	883.6	1.71	25.6
	1033.3	1.66	24.8
	1182.7	1.56	23.4
	1326.0	1.47	22.0
	1465.6	1.44	21.6
	1616.6	1.40	20.9
	1756.3	1.35	20.3
	1894.5	1.26	18.9
	1987.7	1.24	18.6
C (4.2%)	386.8	1.62	32.2
	455.8	1.76	35.1
	522.9	1.79	35.6
	593.7	1.87	37.3
	664.6	1.85	36.9
	737.5	1.88	37.5
	809.9	1.85	36.9
	879.0	1.90	37.9
	959.9	1.80	36.0
	1026.3	1.82	36.2
	1109.2	1.76	35.1
	1172.9	1.72	34.2
	1260.3	1.66	33.1
	1322.1	1.64	32.8
	1403.9	1.59	31.8
	1464.2	1.55	30.9
	1549.9	1.50	29.9
	1608.7	1.51	30.1
	1698.0	1.43	28.5
	1748.9	1.44	28.7
	1836.4	1.35	26.9
	1892.4	1.35	26.9
	1941.5	1.34	26.7
	1990.7	1.33	26.6
Mg (3.8%)	412.0	1.34	56.5
	489.3	1.38	55.6
	557.5	1.42	57.2
	630.9	1.44	58.0
	699.0	1.43	57.9
	791.2	1.41	56.7
	852.7	1.39	56.2
	922.8	1.39	55.9
	989.3	1.40	56.4
	1072.3	1.36	55.1
	1159.6	1.30	52.3
	1224.8	1.34	54.2
	1305.8	1.25	50.6
	1374.4	1.25	50.5
	1451.7	1.21	49.0
	1530.1	1.27	51.4
	1602.3	1.21	48.8
	1672.8	1.20	48.6
	1743.2	1.15	46.2
	1817.7	1.16	47.0
	1891.8	1.15	46.6
	1968.7	1.13	45.7
Al (3.9%)	385.9	1.20	53.8
	449.0	1.22	54.7
	524.5	1.25	55.9
	590.0	1.24	55.5
	661.9	1.21	54.2
	735.9	1.18	52.8
	794.6	1.17	52.3
	831.9	1.22	54.5
	876.0	1.16	51.9
	957.8	1.16	52.1
	1023.8	1.18	52.7
Al (3.9%)	1098.8	1.14	50.9
	1168.6	1.10	49.3
	1260.0	1.12	50.4
	1324.2	1.09	49.0
	1396.1	1.09	49.0
	1461.2	1.06	47.4
	1552.3	1.06	47.3
	1613.4	1.05	47.0
	1701.4	1.05	46.9
	1752.7	1.06	47.3
	1848.1	1.01	45.0
	1904.7	0.974	43.6
Ti (4.1%)	437.2	1.16	92.1
	582.6	1.20	95.2
	723.1	1.20	95.7
	873.0	1.22	96.9
	1018.6	1.15	91.5
	1168.3	1.16	92.1
	1314.4	1.10	87.1
	1459.7	1.06	83.9
	1609.6	0.998	79.4
	1754.3	0.985	78.3
	1901.4	0.930	74.0
	2001.1	0.947	75.3
V (3.7%)	407.8	1.11	94.0
	556.8	1.18	99.4
	688.2	1.18	100.1
	830.2	1.18	100.1
	980.7	1.14	96.2
	1139.6	1.12	94.5
	1273.8	1.10	93.4
	1420.2	1.06	89.5
	1571.2	1.01	85.1
	1729.0	0.970	82.0
	1865.1	0.976	82.5
	1955.9	0.941	79.6
Cr (3.7%)	416.0	0.930	80.2
	570.4	0.973	84.0
	706.8	0.990	85.5
	852.6	1.01	87.2
	998.8	1.01	87.2
	1156.0	0.969	83.6
	1302.8	0.944	81.5
	1452.2	0.926	80.0
	1604.2	0.909	78.4
	1746.9	0.855	73.8
	1865.1	0.829	71.6
	1949.0	0.825	71.2
	2028.7	0.825	71.2
Mn (3.6%)	352.4	0.807	73.6
	412.2	0.869	79.3
	523.0	0.876	79.9
	627.6	0.934	85.1
	698.3	0.920	83.9
	777.9	0.912	83.2
	848.8	0.928	84.6
	920.1	0.930	84.8
	988.7	0.940	85.7
	1102.3	0.885	80.7
	1214.3	0.890	81.2
	1280.6	0.864	78.8
	1398.2	0.856	78.1
	1515.8	0.830	75.7
	1582.6	0.846	77.1
	1690.1	0.805	73.4
	1811.0	0.783	71.4
	1889.1	0.781	71.2
	1962.1	0.792	72.3

TABLE II. (*Continued*)

Stopping material	Energy (keV)	$dE/\rho dx$ (keV cm²/μg)	ϵ (10^{-15} eV cm²)
Fe (3.8%)	431.1	0.927	85.9
	570.3	0.977	90.6
	713.2	1.01	93.1
	856.7	1.02	94.7
	1006.6	1.00	93.0
	1152.3	0.990	91.7
	1300.0	0.955	88.6
	1444.1	0.925	85.7
	1591.2	0.905	83.9
	1739.6	0.847	78.5
	1885.5	0.837	77.6
	1979.2	0.811	75.1
Co (3.8%)	435.6	0.743	72.7
	565.4	0.812	79.5
	718.7	0.838	82.0
	856.7	0.840	82.2
	1008.0	0.838	82.0
	1151.6	0.821	80.3
	1291.5	0.822	80.4
	1447.2	0.782	76.5
	1599.7	0.772	75.5
	1738.6	0.759	74.2
	1896.4	0.730	71.4
	1989.1	0.719	70.3
Ni (3.9%)	433.3	0.707	68.9
	587.0	0.762	74.2
	717.4	0.791	77.0
	863.3	0.813	79.2
	1007.2	0.795	77.4
	1163.7	0.793	77.3
	1299.2	0.780	76.0
	1444.3	0.777	75.7
	1592.2	0.778	75.8
	1748.5	0.747	72.6
	1887.0	0.727	70.9
	1987.5	0.717	69.9
Cu (3.7%)	417.7	0.592	62.4
	571.5	0.648	68.3
	686.7	0.669	70.6
	829.9	0.695	73.3
	966.9	0.675	71.2
	1142.8	0.697	73.5
	1274.8	0.701	73.9
	1420.0	0.691	72.8
	1567.7	0.708	74.7
	1723.0	0.679	71.6
	1863.7	0.662	69.8
	1953.7	0.647	68.2
Ge (4.0%)	441.4	0.765	92.2
	591.5	0.820	98.8
	725.4	0.828	99.8
	870.3	0.820	98.8
	1017.9	0.806	97.1
	1169.1	0.792	95.4
	1308.9	0.777	93.6
	1453.3	0.787	94.8
	1599.9	0.726	87.4
	1747.0	0.721	86.9
	1890.3	0.716	86.3
	1984.1	0.703	84.7
Pd (4.2%)	449.4	0.532	94.2
	581.3	0.579	102.5
	677.1	0.623	110.3
Pd (4.2%)	788.7	0.624	110.5
	933.5	0.640	113.4
	1071.2	0.643	113.9
	1167.5	0.629	111.5
	1261.1	0.612	108.4
	1364.7	0.614	108.7
	1466.8	0.566	100.2
	1550.8	0.587	104.0
	1627.2	0.551	97.5
	1732.5	0.536	95.0
	1839.9	0.529	93.7
	1922.2	0.532	94.3
	2007.1	0.523	92.6
Ag (3.8%)	448.4	0.517	92.4
	585.9	0.571	102.2
	721.4	0.588	105.1
	850.5	0.613	109.7
	1009.1	0.615	110.0
	1143.9	0.611	109.3
	1278.0	0.604	108.1
	1420.5	0.590	105.6
	1571.7	0.567	101.4
	1733.8	0.543	97.1
	1862.0	0.534	95.6
	1961.1	0.509	91.0
In (4.5%)	565.2	0.569	108.4
	693.4	0.602	114.8
	751.0	0.585	111.6
	834.2	0.580	110.6
	891.4	0.566	107.9
	980.0	0.608	115.0
	1038.8	0.591	112.6
	1132.8	0.599	114.1
	1179.1	0.613	116.8
	1274.6	0.595	113.4
	1329.2	0.614	117.0
	1417.8	0.574	109.3
	1471.1	0.594	113.2
	1561.1	0.577	110.1
	1709.3	0.555	105.8
	1846.9	0.527	100.5
	1945.1	0.521	99.2
Sn (3.7%)	375.6	0.541	106.5
	436.5	0.555	109.3
	508.5	0.577	113.7
	572.8	0.590	116.2
	652.1	0.595	117.2
	720.4	0.589	116.1
	796.1	0.611	120.4
	864.2	0.604	119.0
	938.1	0.603	118.8
	1006.0	0.600	118.2
	1088.0	0.592	116.6
	1156.2	0.586	115.5
	1234.8	0.585	115.3
	1298.3	0.578	113.8
	1389.4	0.570	112.3
	1445.2	0.557	109.7
	1529.7	0.566	111.5
	1590.6	0.549	108.1
	1679.8	0.544	107.2
	1744.0	0.526	103.7
	1825.2	0.522	102.9
	1926.4	0.515	101.5

parameters A and B and the region of validity of the curve are given in Table III for each stopping element.

In Fig. 2 the agreement between Whaling's estimate (±20%) and the present measurements in Be is from 8% at the low-energy end to 13% at the high-energy

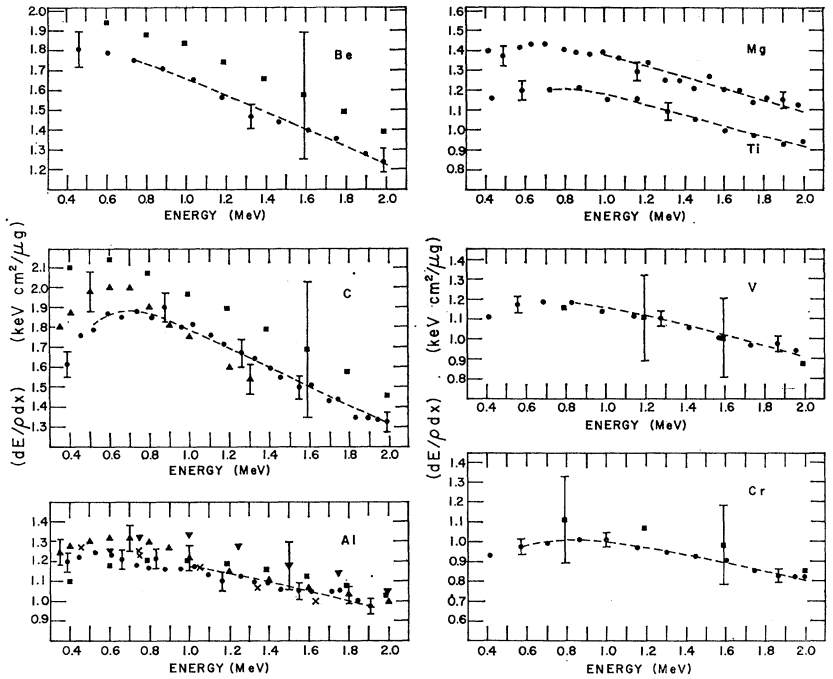

FIG. 2. Energy loss of α particles versus energy in Be, C, Al, Mg, Ti, V, and Cr. The present measurements (± 3.6 to 4.9% accuracy) are given by the dark circles. The ×'s are the 60° magnetic spectrometer test measurements (see text) of the present experiment in Al. The triangles are the measurements ($\pm 5\%$ accuracy) of Porat and Ramavataram. The inverted triangles ($\pm 10\%$ accuracy) are due to Gobeli, and the squares ($\pm 20\%$ accuracy) are estimates by Whaling from proton-stopping cross-section measurements. The dashed line is a least-squares curve fit to a portion of the present measurements (the equation and curve-fitted parameters are given in Table III).

end. Porat and Ramavataram's measurement in C at 0.4 MeV is 15% higher than the present measurement and at 1.3 MeV is 6% lower than the present measurement, with the crossover occurring at 0.88 MeV. Whaling's estimate of $dE/\rho dx$ in C are from 9 to 20% higher than the present measurements. The reason for the disagreement among the measurements is unknown. The present C measurements are reproducible with four different target thicknesses. Between two of the C $dE/\rho dx$ measurements, an Ag target was inserted in the scattering chamber, and $dE/\rho dx$ measurements of α particles in Ag were made. It is seen in Fig. 3 that the Ag measurements by all groups are in excellent agreement. When the C measurement was repeated at all α energies with a different target thickness from that used before the Ag measurement, the same result in C

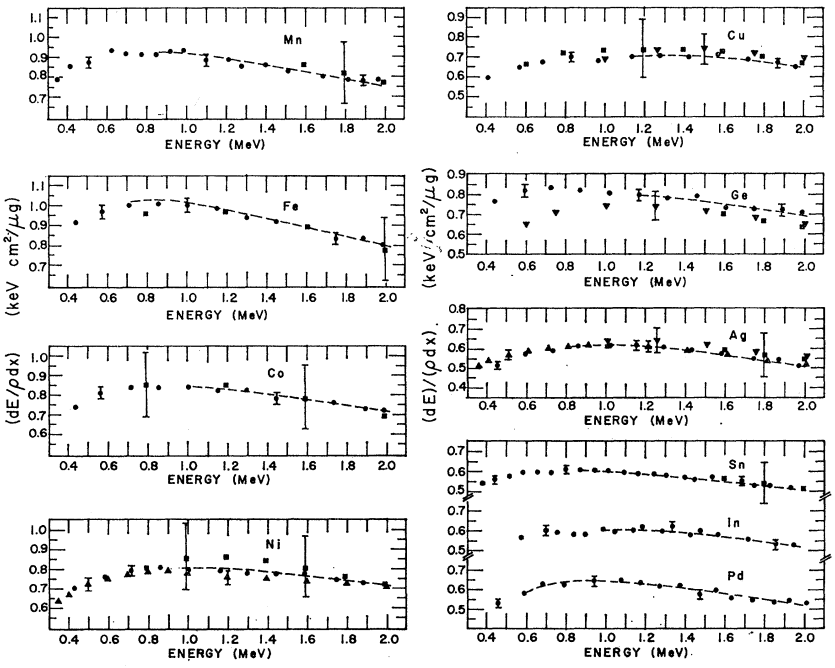

FIG. 3. Energy loss of α particles versus energy in Mn, Fe, Co, Ni, Cu, Ge, Ag, Pd, In, and Sn. The present measurements (± 3.6 to 4.9% accuracy) are given by the dark circles. The triangles are the measurements ($\pm 5\%$ accuracy) of Porat and Ramavataram. The inverted triangles ($\pm 10\%$ accuracy) are due to Gobeli, and the squares ($\pm 20\%$ accuracy) are estimates by Whaling from proton-stopping–cross-section measurements. The dashed line is a least-squares curve fit to a portion of the present measurements (the equation and curve-fitted parameters are given in Table III).

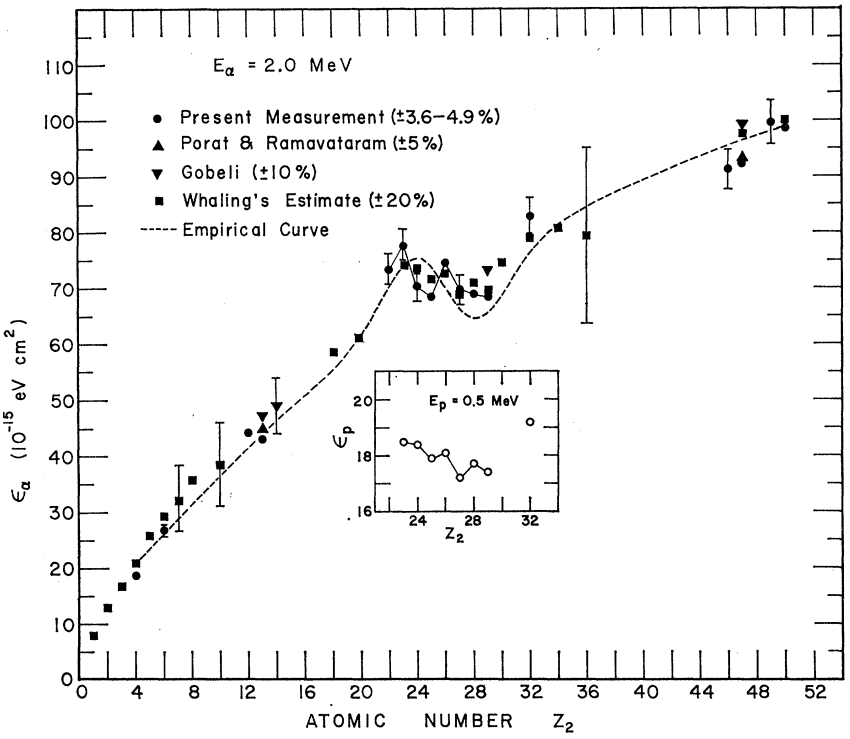

FIG. 4. Stopping cross section ϵ_α of α particles versus the stopping element atomic number Z_2 at E_α=2.0 MeV. Present measurements (●; ±3.6 to 4.9% accuracy), Porat and Ramavataram's measurements (▲; ±5% accuracy), Gobeli's data (▼; ±10% accuracy), and Whaling's estimates (■; ±20% accuracy) from proton-stopping measurements. A solid line is used to connect the ϵ_α measurement in the range Z_2=22–29 to show the structure of ϵ_α in Z_2. The dashed line is an empirical formula $\epsilon_\alpha(E_\alpha,Z_2)$ (see text) obtained from the present measurements. The small figure is the proton-stopping cross section ϵ_p versus Z_2 for E_p=0.5 MeV, Z_2=23–32 (see Ref. 22). Units on the ordinate are the same in the small and large figures.

was obtained as before the Ag measurement. Porat and Ramavataram's measurements in Al are about 5% higher at the low-energy end and about 3% higher at the high-energy end than the present measurements in Al. At 0.6 MeV Gobeli's measurement in Al agrees with the present measurement, but his data at other energies are 9–14% higher than the present measurements. Whaling's estimate in Al is about 9% lower at the low-energy end and 8% higher than the present measurements at the high-energy end.

The agreement between Whaling's estimate in V and the present measurement in V is within 3%. In Cr his estimate at 0.79 MeV is about 10% higher and at 2 MeV is 5% higher than the present measurements. In Fig. 3 the agreement between his estimate in Mn and the present measurement in Mn is within 5%. His estimate agrees with the present measurement in Fe to within 5%. In Co the agreement is within experimental accuracy.

The present measurements in Ni agree within experimental accuracy with Porat and Ramavataram's measurements. At 1.2 MeV Porat and Ramavataram's measurement is 5% lower and Whaling's estimate is 10% higher than the present measurement. Gobeli's $dE/\rho dx$ in Cu agrees with the present measurementa at 1 MeV but is about 10% higher at 2 MeV. Whaling's estimates are from 4 to 7% higher than the present measurements in Cu. His estimate in Ge is available only above 1.59 MeV and is 6% lower at 2 MeV than the present measurement in Ge.

The present measurements of $dE/\rho dx$ of α particles in Pd, In, and Sn are plotted in Fig. 3. Whaling's estimate is available only for Sn as a stopping element, and is in good agreement with the present Sn measurements.

VII. DISCUSSION

An attempt has been made to see whether a systematic relation exists between ϵ_α and the atomic number Z_2 of the stopping elements in the energy region 0.4

TABLE III. Curve-fitted parameters for $dE/\rho dx=(A/E)\times\ln(BE)$ of α particles in solids as a function of energy. $E_b\leqslant E\leqslant 2.0$ MeV. The fitted curves are plotted in Figs. 2 and 3. E_b represents the lowest energy for which the curve fit applies.

Stopping material	A (keV cm^2/μg MeV)	B (MeV^{-1})	E_b (MeV)
Be	1.175	4.12	0.75
C	1.290	3.98	0.55
Mg	1.167	3.26	1.00
Al	1.007	2.97	1.00
Ti	0.955	3.45	0.75
V	0.965	3.34	0.80
Cr	0.894	3.08	0.60
Mn	0.836	3.01	0.90
Fe	0.846	3.33	0.70
Co	0.838	2.73	1.00
Ni	0.872	2.53	1.00
Cu	0.891	2.15	1.15
Ge	0.810	2.73	1.10
Pd	0.568	3.08	0.60
Ag	0.594	2.83	0.80
In	0.642	2.55	0.95
Sn	0.572	2.88	0.85

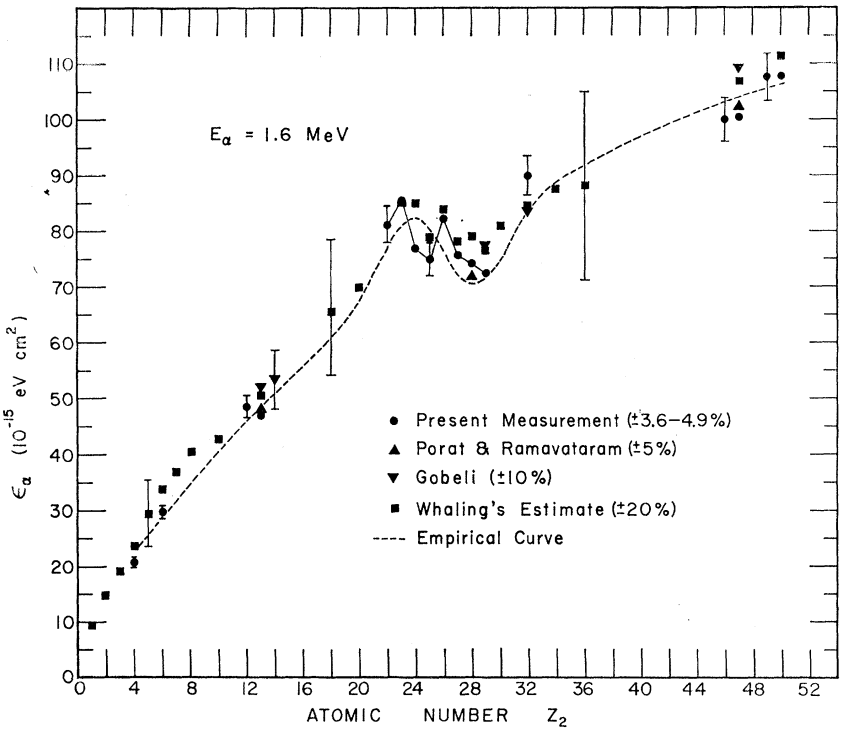

FIG. 5. Stopping cross section ϵ_α of α particles versus the stopping element atomic number Z_2 at $E_\alpha = 1.6$ MeV. Present measurements (●; ±3.6 to 4.9% accuracy), Porat and Ramavataram's measurements (▲; ±5% accuracy), Gobeli's data (▼; ±10% accuracy), and Whaling's estimates (■; ±20% accuracy) from proton-stopping measurements. A solid line is used to connect the ϵ_α measurement in the range $Z_2 = 22$–29 to show the structure of ϵ_α in Z_2. The dashed line is an empirical formula $\epsilon_\alpha(E_\alpha, Z_2)$ (see text) obtained from the present measurements.

$\leq E \leq 2$ MeV. For α particles in this energy region the stopping process is complicated by two considerations: (1) The α-particle effective charge, which is a function of the energy, has a value between roughly 1 and 2; (2) the velocity of the α particles is of the order of the velocity of the orbital electrons of the stopping element;

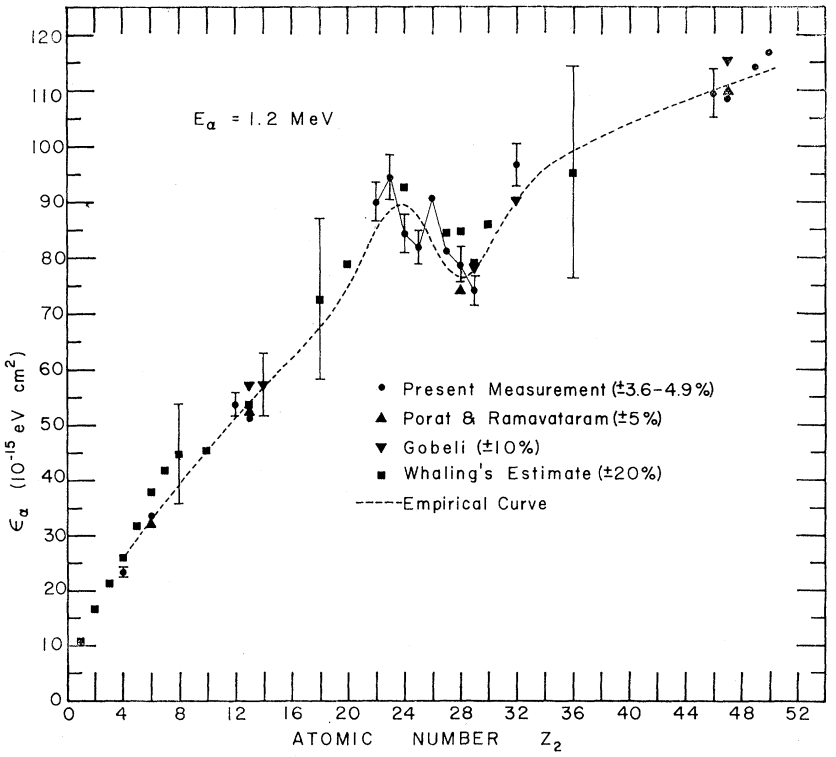

FIG. 6. Stopping cross section ϵ_α of α particles versus the stopping element atomic number Z_2 at $E_\alpha = 1.2$ MeV. Present measurements (●; ±3.6 to 4.9% accuracy), Porat and Ramavataram's measurements (▲; ±5% accuracy), Gobeli's data (▼; ±10% accuracy), and Whaling's estimates (■; ±20% accuracy) from proton-stopping measurements. A solid line is used to connect the ϵ_α measurement in the range $Z_2 = 22$–29 to show the structure of ϵ_α in Z_2. The dashed line is an empirical formula $\epsilon_\alpha(E_\alpha, Z_2)$ (see text) obtained from the present measurements.

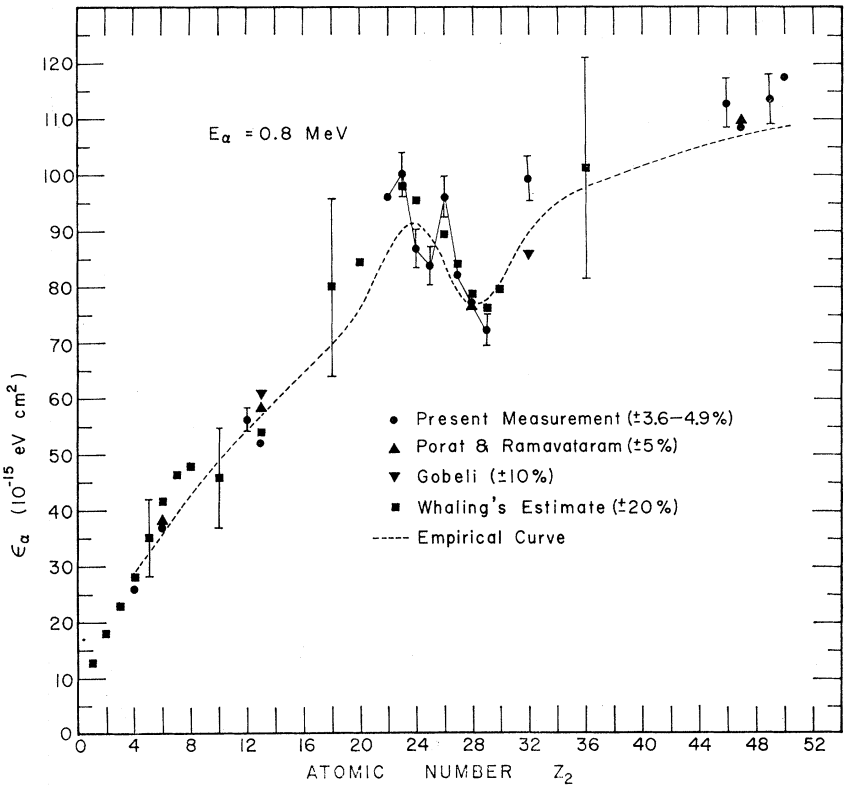

FIG. 7. Stopping cross section ϵ_α of α particles versus the stopping element atomic number Z_2 at $E_\alpha = 0.8$ MeV. Present measurements (●; ±3.6 to 4.9% accuracy), Porat and Ramavataram's measurements (▲; ±5% accuracy), Gobeli's data (▼; ±10% accuracy), and Whaling's estimates (■; ±20% accuracy) from proton-stopping measurements. A solid line is used to connect the ϵ_α measurement in the range $Z_2 = 22$–29 to show the structure of ϵ_α in Z_2. The dashed line is an empirical formula $\epsilon_\alpha(E_\alpha, Z_2)$ (see text) obtained from the present measurements.

in this velocity region neither the adiabatic nor the sudden approximation can be applied for constructing a quantum-mechanical theory of the energy-loss problem. There is no theoretical calculation available at present for α particles in this energy region. ϵ_α versus Z_2 for $E_\alpha = 2.0$, 1.6, 1.2, and 0.8 MeV is given in Figs. 4, 5, 6, and 7, respectively. The closed circles are the ϵ_α either obtained from the curve fit (see Table III) to the present experimental data, or are interpolated from the present experimental measurements. The dotted curve is an empirical formula based on the measurements of this experiment, and will be discussed later.

In Figs. 4–7, ϵ_α increases with the atomic number of the stopping material Z_2, except in the region $Z_2 = 22$–29 (Ti to Cu) where a zigzag exists, and where ϵ_α decreases with increasing Z_2 except at $Z_2 = 26$, which is higher than neighboring Z_2 values. A plot of proton stopping cross section[22] ϵ_p in $Z_2 = 23$–29 ($Z_2 = 22$ information is not available) reveals a similar dependence of ϵ_p with Z_2 (see, for example, Fig. 4, where ϵ_p is plotted at $E_p = 0.5$ MeV; protons of this energy have the same velocity as α particles at 2.0 MeV). The zigzag and decrease of ϵ_α with Z_2 in the region $Z_2 = 22$–29 is definitely outside the present experimental error, particularly at the lower α energies. The observation of the same effect in proton stopping cross sections,[22] as seen in Fig. 4, gives strong support to the reality of the present findings. It is also seen from Figs. 4–7 that the amplitude of the zigzag and the decrease of ϵ_α with Z_2 in the range $Z_2 = 22$–29 are distinctly energy-dependent. Both effects are more pronounced at 800 keV than at 2 MeV, and there appears to be a diminishing of the effect with increasing ion energy.

At higher energies (considerably higher velocities than those of the present measurements) Andersen *et al.*[23] report the energy loss of protons in the $Z_2 = 20$–30 region for $E_p = 2.25$–12 MeV, but the above-mentioned zigzag and the decrease of ϵ_p on Z_2 are not explicit in their measurements. For proton energies above 5 MeV, Mackenzie[24] reports a structure in ϵ_p versus Z_2, especially in the transition elements from Ca to Ni.

Ormrod and Duckworth[1] noticed that there was a periodic variation of ϵ_{ion} with the atomic number Z_1 of the projectile. Fastrup and co-workers obtained a similar periodic variation of ϵ_{ion} with the atomic number of the projectiles $6 \leq Z_1 \leq 20$ in C films[6] from 0.1 to 1.0 MeV and from $21 \leq Z_1 \leq 39$ in C films[7] from 0.2 to 1.5 MeV, and they also observed that the relative amplitude of the oscillations tended to decrease with increasing particle velocity, which they attributed as possibly due to shell effects averaging out as a result of more close collisions when the electron clouds penetrate each other more deeply. A calculation of the minimum distance of

[23] H. H. Andersen, C. C. Hanke, H. Simonsen, H. Sørensen, and P. Vajda, Phys. Rev. **175**, 389 (1968); H. H. Andersen, H. Sørensen, and P. Vadja, *ibid.* **180**, 373 (1969).

[24] K. R. Mackenzie, in *Penetration of Charged Particles in Matter*, edited by Edwin A. Uehling (National Academy of Sciences—National Research Council, Washington, D. C., 1960).

approach in a Coulomb collision, however, reveals that even at very low ion velocities, the electron clouds are already deeply penetrating each other.

Ericksson *et al.*[8] obtained the electronic stopping powers at a constant velocity of 1.5×10^8 cm/sec for 13 different ions in an oriented W single crystal by differentiating their range measurements. A periodic dependence of electronic stopping cross section upon Z_1 was observed. Eisen[9] obtained electronic stopping powers for $5\leq Z_1\leq 19$ in single Si crystals at $V=1.5\times10^8$ cm/sec and also observed an oscillating dependence of ϵ_{ion} with Z_1.

In the low-velocity region (the region where the measurements of Ormrod, Fastrup, Eriksson, Eisen, and co-workers are applicable, and the region of lower velocities than those of the present experiment) Firsov's theory[10] suggests that the energy transfer during the collision between the incoming ion and the stopping atom depends on the square ϕ^2 of the potential between the two interacting atoms. $\phi(r)$ is obtained by the addition of the individual atomic potentials at one-half the separation distance r between the two atoms. The larger the ϕ^2, the larger is the energy transfer, and, consequently, the larger the stopping effect. By introducing the effective charge due to shell effects into the Firsov theory, El-Hoshy and Gibbons[13] have produced an oscillatory structure of $\phi(r)$ to give an explanation of the periodic oscillation of the electronic stopping cross section versus Z_1 in the low-velocity region. Their calculation agrees well with the W channeling experiment of Eriksson and co-workers.[8]

El-Hoshy and Gibbons[13] in their Fig. 10 give various types of binary interaction (Thomas-Fermi, Firsov, Hartree-Fock-Slater, and modified Firsov) between an atom of atomic number Z_1 and a Si atom at a separation $r=3$ a.u. They indicate that the Hartree-Fock-Slater potential is higher in value than the Thomas-Fermi potential and the Firsov potential, and also that the Hartree-Fock-Slater potential displays a structure missing from the other potentials. They state that the actual physical potential should be similar to the Hartree-Fock-Slater potential in structure but higher in magnitude because of a partial depletion of the electrons in the space between the two atoms. They obtain the modified Firsov potential by using the effective charge of the atoms and by varying the interaction radius between the interacting atoms.

Unfortunately, the theory of Firsov as modified by El-Hoshy and Gibbons,[13] by Winterbon,[12] or by Cheshire *et al.*,[12] or the Lindhard theory as modified by Bhalla and Bradford,[12] to predict the oscillatory dependence upon Z_1 cannot be applied to the present experiment (where the effect of ϵ_α upon Z_2 was studied) because the present measurements are made in a higher velocity region, where the theory does not apply. Also, the present measurements are below, or just into, the even higher velocity region where the Bethe-Bloch formalism applies (as, for example, in the region of Andersen's measurements). The dependence of the Bethe-Bloch formula upon the interacting potential between the incoming ion and the stopping electron (Z_1e^2/r) leads to a dE/dx proportional to $Z_1^2Z_2$. The Z_1^2 arises from the square of a momentum impulse[25] $[\Delta P\sim Z_1\sim\int(Z_1e^2/r)dt]$ transferred to the stationary electron, i.e., the square of the integral of the Coulomb potential. The Z_2 arises from the fact that there are Z_2 electrons per stopping atom.

From the above considerations the dependence in the low-velocity region of dE/dx on the potential ϕ in Firsov's theory is through an integral of ϕ^2, and the dependence of dE/dx in the high-velocity region on the Coulomb potential Z_1e^2/r is through the square of an integral of Z_1e^2/r. It is then not unreasonable to assume for qualitative discussion that in the intermediate-velocity region the interaction potential enters into the stopping-cross-section calculation in a way similar to that in the other velocity regions. That is to say, the dependence of dE/dx on Z_1 or Z_2 is similar to the dependence of the interaction potential on Z_1 or Z_2 through some power or function of this potential. Changes of the potential with Z_1 or Z_2 will then show up as changes of dE/dx with Z_1 or Z_2.

To connect the structure of the Hartree-Fock-Slater potential to the present experimental measurements, we refer to Bohm's statement[26] that the energy transfer during a collision will be a maximum at some projectile velocity of the order of the velocities of electrons in the target atoms. In the present experiment the energy $E_\alpha=0.4$–2.0 MeV corresponds to an α-particle velocity $V_\alpha=4.4\times10^8$ to 9.8×10^8 cm/sec.

The velocity of the electrons in the target atom can be determined from the x-ray energy spectrum for a given atom. For $Z=22$–30, the velocities of the orbital electrons of different shells are $V_K=40\times10^8\sim60\times10^8$ cm/sec, $V_L=12\times10^8\sim20\times10^8$ cm/sec, and $V_M\lesssim8\times10^8$ cm/sec. The velocity V_N of the outermost shell is uncertain from x-ray data, but ionization-potential data indicate that $V_N\approx1.7\times10^8$ cm/sec.

If the charge density of the atom is plotted as a function of the radius of the atom, several peaks may be seen in the resulting plot. We have taken the radius of the subshell corresponding to the peak of maximum height as an estimate of the radius of each shell. The peak of maximum height is obtained from the Hartree-Fock-Slater radial-wave-function tabulation of Herman and Skillman.[27] For $Z=22$–30 the radius of each shell is $r_K\approx0.03\sim0.045$ a.u., $r_L\approx0.15\sim0.3$ a.u., $r_M\approx0.5\sim1.0$ a.u., and $r_N\approx2\sim3$ a.u.

We would expect the energy transfer of the α particles of 0.4–2.0 MeV to have a greater significance in the

[25] W. Whaling, in *Nuclear Spectroscopy*, edited by F. Ajzenberg-Selove (Academic Press Inc., New York, 1960), Part A, p. 3.

[26] D. Bohm, *Quantum Theory* (Prentice-Hall, Inc., Englewood Cliffs, N. J., 1951), p. 506.

[27] F. Herman and S. Skillman, *Atomic Structure Calculations* (Prentice-Hall, Inc., Englewood Cliffs, N. J., 1963).

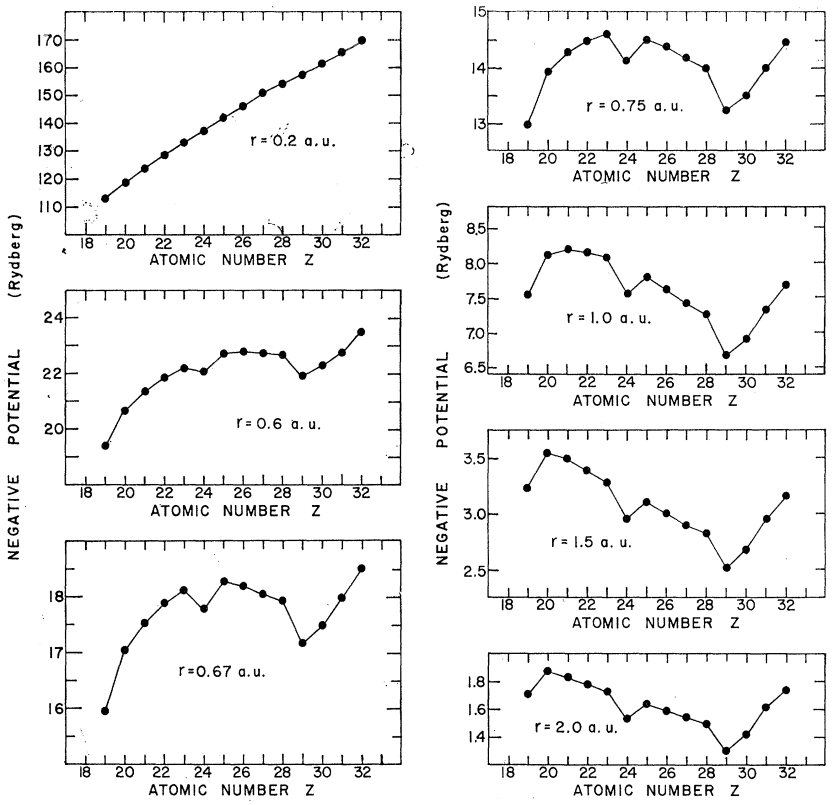

FIG. 8. The negative atomic potential energy $\phi(r)$ (in Ry) versus Z as determined by a Hartree-Fock-Slater calculation (Ref. 27) at various radii (in a.u.). The solid line is used to connect the points to emphasize the structure.

M shell for the $Z_2=22$–30 region based on a comparison of the incoming α-particle velocity to the velocity of the orbital electrons of the target atoms. This is not to say that the other electrons of the stopping atom have no effect on the stopping process. The binding energy of the electrons plays a part in the stopping process; the outermost electrons are stripped off more easily than the innermost electrons, but the energy transfer is greater to those electrons whose velocity is of the same magnitude of the ion velocity.

In Fig. 8 the Hartree-Fock-Slater potentials from Herman and Skillman's tabulation[27] at different radii are plotted as a function of Z. The interacting potential between the α particles and the stopping atoms will have the same Z_2 dependence as in Fig. 8, except that the potential will be offset by the potential due to the α particle. The shape of the Hartree-Fock-Slater potential at $r=1.5$ a.u. is different from that of El-Hoshy and Gibbons (Figs. 5 and 10 of Ref. 11) which we suspect to be due to a plotting mistake in the region of $Z=26$–28.

Comparison can be made between Figs. 4–7 and Fig. 8 as follows: For ϵ_α at $E_\alpha=2$ MeV, V_α corresponds to ϕ at $r=0.6$ a.u.; for ϵ_α at $E_\alpha=0.8$ MeV, V_α corresponds to ϕ at $r=0.75$ a.u.; and for ϵ_α at $E_\alpha=1.2$ and 1.6 MeV, V_α corresponds to ϕ at $r\approx0.67$ a.u. The energy E_α and the stopping electron orbital radius r are related by a velocity comparison between the projectile and the orbital electrons of the target element. One can see a similarity in structure between $\epsilon_\alpha(E_\alpha)$ versus Z_2 and $\phi(r)$ versus Z. That is to say, from $Z=22$ to $Z=29$ there is a decreasing interaction potential with increasing Z, and our measurements indicate a decreasing ϵ_α with Z_2 in the same Z_2 region. It is also seen in our Figs. 4–7 that there are always two dips, one at Mn ($Z=25$) and the other at Cu ($Z=29$). At $Z=24$ the Cr measurement is also low, so that it could be a dip within the experimental accuracy. The two dips at $Z=24$ and 29, as predicted by $\phi(r)$ in Fig. 8, can be explained, since at $Z=24$ and 29 there is only one electron in the $4s$ shell compared to two $4s$ electrons for the other elements in the region $Z=22$–30. The present experiment gives a peak at Fe ($Z=26$), but no peak at Fe is predicted by the Hartree-Fock-Slater two-atom potential. The comparison between $\epsilon_\alpha(E_\alpha)$ versus Z_2 and $\phi(r)$ versus Z by relating E_α to r using Bohm's statement gives a qualitative explanation of the cause of the structure in ϵ_α versus Z_2 and also gives the energy dependence of the amplitude of the structure which decreases with increasing ion energy corresponding to a smaller radius of interaction.

At present a quantitative explanation of our measurements is beyond our reach because of two complications: (1) The real atom does not have a well-defined orbital radius for its shell electrons, and (2) the formalism for the energy loss in the intermediate-velocity region is not developed to show precisely how $\phi(r)$ enters into the calculation of ϵ.

In Fig. 8, $\phi(r)$ at $r=2.0$, 1.5, and 0.2 a.u. is also plotted. Large r corresponds to maximum interaction with a slow projectile, and the structure of $\phi(r)$ on Z is more pronounced. Small r corresponds to fast projectiles, and $\phi(r)$ becomes a monotonic function of Z. At $r=0.2$ a.u. (about the radius of the L shell for $Z=20$–30), the orbital electrons have velocity about 10–20×10^8 cm/sec, which corresponds to $E_p\approx2$ MeV, the lower limit of Andersen's measurements of ϵ_p ($E_p=2.25$–12 MeV). No structure is seen in either ϵ_p versus Z_2 or in $\phi(r)$ versus Z. This result is not inconsistent with the qualitative discussion given herein. Of course, it should be understood that, in this high-velocity region, the interaction occurs not through a Hartree-Fock-Slater picture of the stopping atom, but rather through the Coulomb force between the incident ion of charge Z_1e and one of the Z_2 electrons of the stopping atom. The Bethe-Bloch formula based on this Coulomb interaction leads to a linear relation between ϵ and Z_2.

To conclude the present discussion, we list the following:

(1) The present experiment confirms that there is a structure in ϵ_α versus Z_2, and that the amplitude of this structure is energy-dependent.

(2) A structure in ϵ_p versus Z_2 in the intermediate region is observed (see Bader *et al.*[20] and Green *et al.*[20]; see also Fig. 4, where ϵ_p is plotted versus Z_2; the structure in ϵ_p is actually more pronounced at lower proton velocities, although these ϵ_p's are not directly plotted in Figs. 5–7).

(3) A Hartree-Fock-Slater potential can be used to explain the structure of ϵ versus Z and the energy dependence of the amplitude of the structure.

At the present time, for convenience in interpolating the stopping cross section for α particles, ϵ_α, to stopping elements not yet measured, an empirical formula based on the present measurements only is given:

$$\epsilon_\alpha=\epsilon_\alpha(E,Z_2)=(A'/E)\ \ln(B'E)\ \text{for}\ 0.8\leq E\leq2.0\ \text{MeV},$$

$4\leq Z_2\leq50$, where E is in MeV, and ϵ_α is in 10^{-15} eV cm^2. The parameter A' and B' are functions of Z_2:

$$B'=5.63Z_2^{-0.2},\quad A'=A_s'+A_w',$$

with

$$A_s'=-0.0132Z_2^2+2.04Z_2+3.40,$$

$$A_w'=-4.0(Z_2-26)\exp[-(Z_2-26)^2/14].$$

A_s' is a monotonic function of Z_2 and A_w' represents a wiggle centered at $Z_2=26$ with its width an adjusted parameter equal to 14 and its amplitude an adjusted parameter equal to 4.0. This empirical formula is plotted as the dashed curve in Figs. 4–7.

In using the above formula the following must be borne in mind: (1) If a target element is measured in the present experiment, Table III is recommended for the ϵ_α evaluation with an accuracy within the experimental error. (2) All the present measurements are within $\pm15\%$ of the curve, 80% of the present measurements are within $\pm10\%$ of the curve (see Figs. 4–7), and all ϵ_α measurements by other groups are within 15% of the curve. (3) Knowing that Ormrod *et al.* and Fastrup *et al.* obtain a periodic oscillation of ϵ_{ion} versus Z_1 for $Z_1\leq20$ with low-velocity ions, and noticing that ϵ_p versus Z_2 has similar structure around $Z_2=7$ (see Figs. 4–7), one may suspect that there would be oscillations in ϵ_α versus Z_2 for Z_2 not included in the present measurement. (4) On the basis of (2) and (3) a 20% accuracy is assigned to the empirical curve. (5) The empirical curve can be improved and modified later as more ϵ_α-versus-Z_2 information becomes available, and if wiggles are observed in some other Z_2 region, the empirical formula should be modified to include more terms similar to A_w'.

ACKNOWLEDGMENTS

We would like to thank Dr. D. L. Hardcastle for several discussions on the application of the Hartree-Fock-Slater potential to the present problem; Dr. K. H. Wang for discussions on the experimental technique and his help in testing the detecting system; and Roy Brown for constructing and testing the electronics used in this experiment.